Supplementary Information for the manuscript

Drivers and mechanisms contributing to excess warming in Europe during recent decades

Buwen Dong[1]* and Rowan T. Sutton[1]

[1] National Centre for Atmospheric Science, Department of Meteorology, University of Reading, Reading, United Kingdom

*corresponding author: Buwen Dong, b.dong@reading.ac.uk

Content:

Supplementary Table S1: CMIP6 and DAMIP models used in this study.

	Model	Resolution (grid number in lat×lon)	Members			
			All	GHG	AER	NAT
1	ACCESS-CM2	145×192	1	3	3	3
2	ACCESS-ESM1-5	144×192	1	1	1	1
3	BCC-CSM2-MR	160×320	3	3	3	3
4	CanESM5	64×128	25	10	10	10
5	CESM2	192×288	6	3	1	3
6	CNRM-CM6-1	128×256	10	10	10	10
7	GFDL-ESM4	180×288	1	1	1	1
8	GISS-E2-1-G	90×144	10	5	5	0
9	HadGEM3-GC31-LL	145×192	4	4	4	4
10	IPSL-CM6A-LR	143×144	9	10	10	10
11	MIROC6	128×256	10	3	3	3
12	MRI-ESM2-0	160×320	5	3	3	3
13	NorESM2-LM	96×144	3	3	3	3
	All models		88	59	57	54

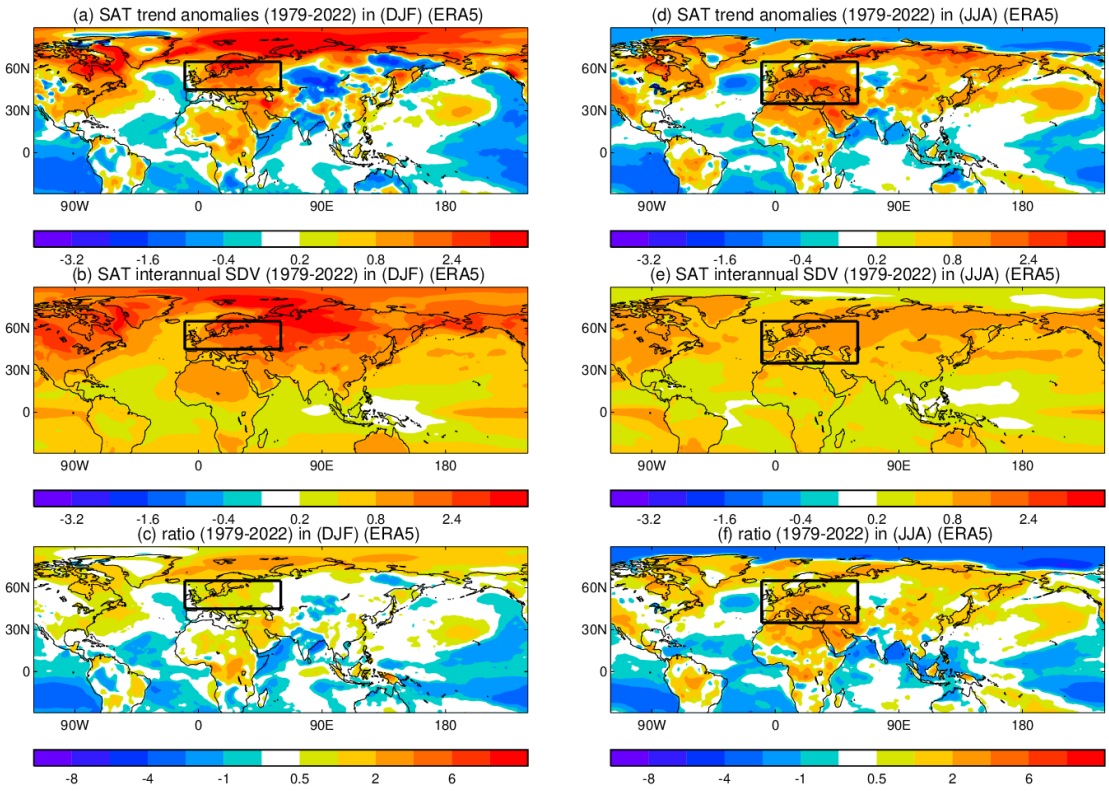

Supplementary Fig. S1: The excess warming trends of SAT, interannual standard deviation of detrended SAT, and their ratios in winter (December, January, February) and summer (June, July, August) based on the ERA5 reanalysis during 1979-2022. (a, d) the excess warming trends of SAT (°C), (b, e) interannual standard deviation of detrended SAT, and (c, f) their ratios. The black box outlines the region that is used to define SAT index over Europe.

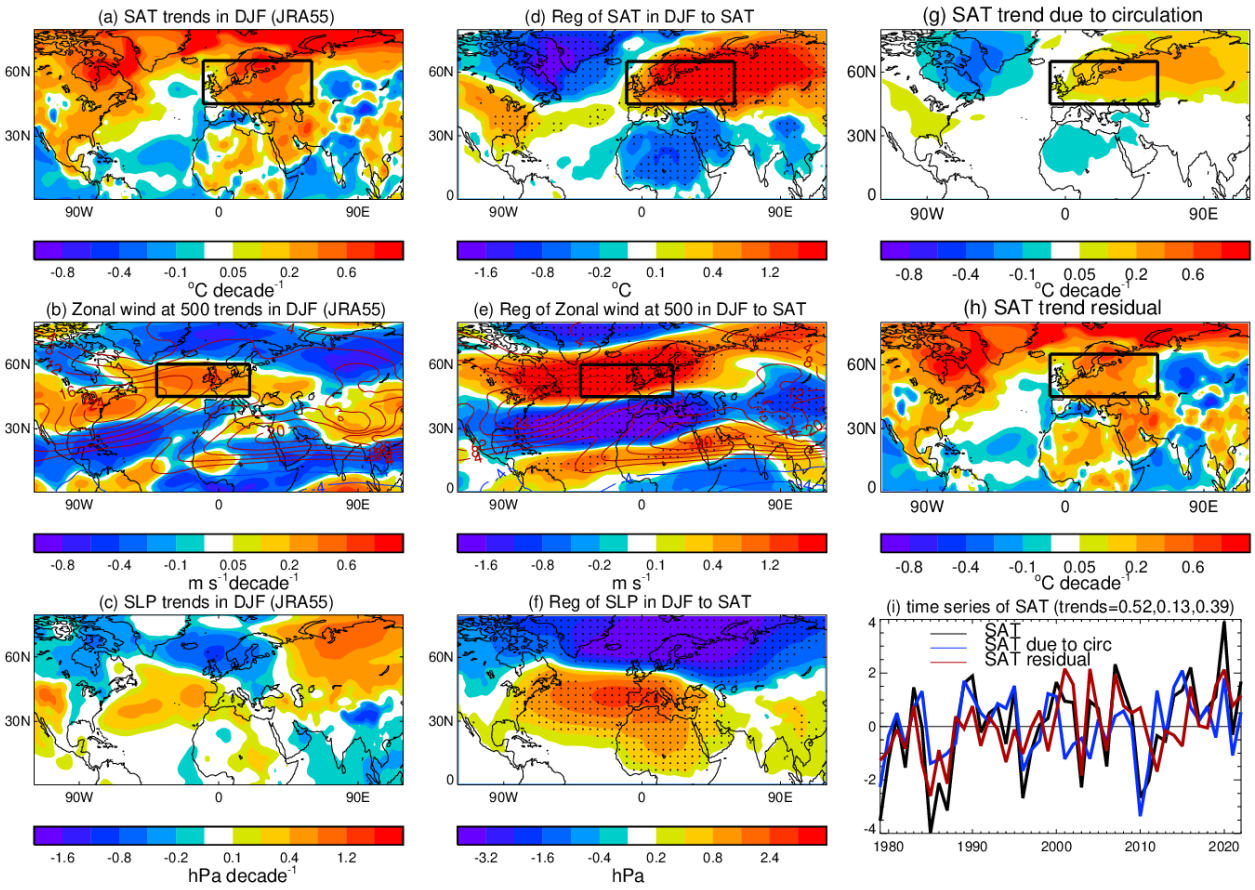

Supplementary Fig. S2: **Linear trends of SAT, atmospheric circulation, regression patterns and circulation induced SAT trends in DJF based on JRA55 reanalysis during 1979-2022.** (a, b, c) Linear trends of SAT (ºC decade-1), zonal wind (m s^{-1} $decade^{-1}$), and SLP (hPa $decade^{-1}$). (d, e, f) Regression patterns of SAT (ºC), zonal wind (m s^{-1}) at 500 hPa, and SLP (hPa) in DJF to the normalized time series of European SAT index which is defined as the area averaged SAT over the region (45ºN-65ºN, 10ºW-60ºE, black box in a, d, g, h) in DJF with detrended data. (g, h) Linear trends of SAT due to circulation changes (ºC $decade^{-1}$) and SAT residual trend (ºC $decade^{-1}$). (i) Time series of SAT anomalies (black), relative contributions due to circulation changes (blue) and residuals (red) over Europe and linear trends (ºC $decade^{-1}$; numbers in top right). The circulation index used for decomposition of SAT trends is the NAO index, defined as the difference of area averaged SLP over the southern box (36ºN-38ºN, 28ºW-22ºW) around Azores and the northern box (64ºN-66ºN, 26ºW-21ºW) around Iceland (see Methods). The global mean is removed in panels (a-h) and the removal of global mean has a very little impact on panels (b-g). Note that nonlinear color bar is used in all spatial patterns.

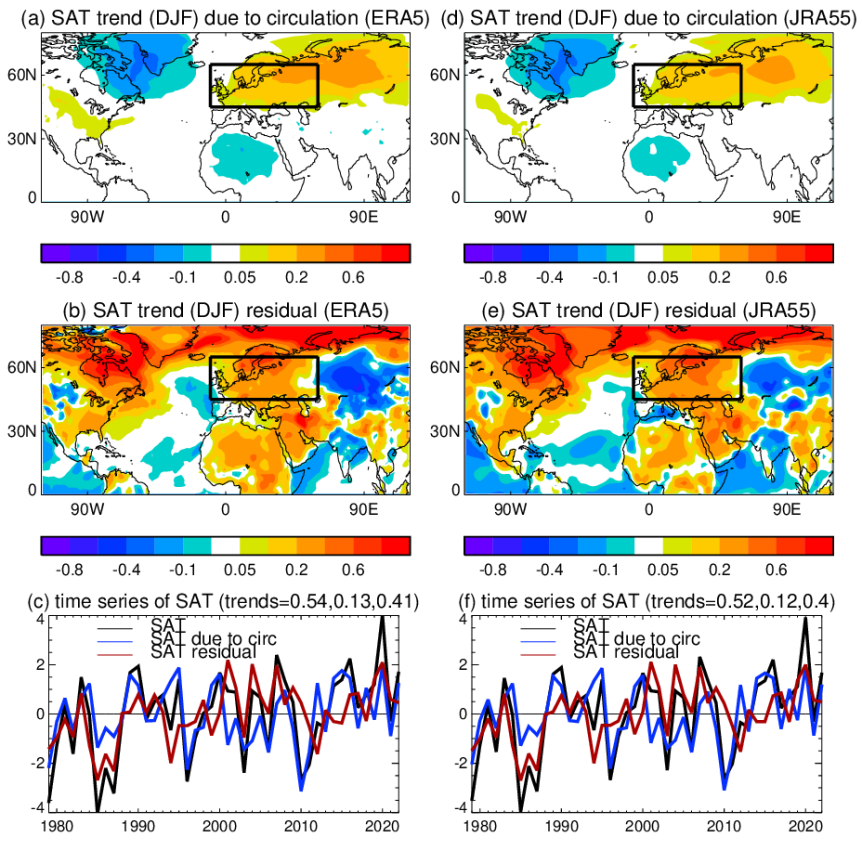

Supplementary Fig. S3: Linear trends of SAT due to circulation changes (based on a zonal wind index) and SAT residual trend in DJF during 1979-2022. (a, d) SAT due to circulation changes (^{o}C decade^{-1}), (b, e) SAT residual trend (^{o}C decade^{-1}), and (c, f) time series of SAT anomalies (black), relative contributions due to circulation changes (blue) and residuals (red) over Europe and linear trends (^{o}C decade^{-1}; numbers in top right). (a, b, c) ERA5 reanalysis and (d, e, f) JRA55 reanalysis. The global mean is removed in panels (a-e) and the removal of global mean has a very little impact on panels (a, e). Note that nonlinear color bar is used in spatial patterns (a-e). The circulation index is a zonal jet index averaged over the North Atlantic jet exit region (45^{o}N-60^{o}N, 50^{o}W-20^{o}E) at 500 hPa which is shown in black box in panels (b, e) in Fig. 2. The black box outlines the region that is used to define SAT index over Europe. The details for decomposition of SAT trends are in Methods.

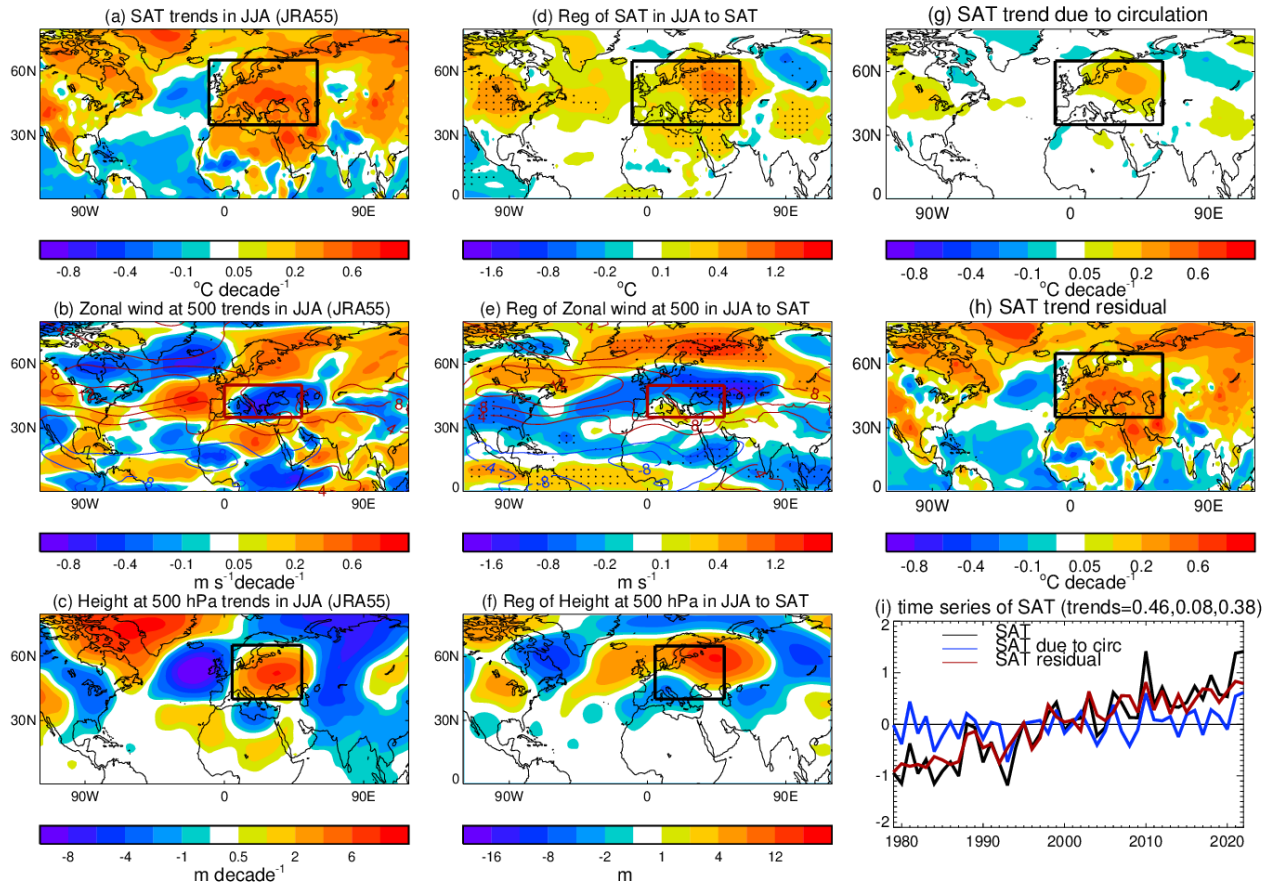

Supplementary Fig. S4: Linear trends of SAT, atmospheric circulation, regression patterns and circulation induced SAT trends in JJA based on JRA55 reanalysis during 1979-2022. (a, b, c) Linear trends of SAT (ºC decade^{-1}), zonal wind (m s^{-1} decade^{-1}) and geopotential height (m decade^{-1}) at 500 hPa. (d, e, f) Regression patterns of SAT (ºC), zonal wind (m s^{-1}) and geopotential height (m) at 500 hPa in JJA to the normalized time series of the European SAT index which is defined as area averaged SAT over the region (35ºN-65ºN, 10ºW-60ºE, black box in a, d, g, h) in JJA with detrended data. (g, h) SAT trends due to circulation changes (ºC decade^{-1}) and SAT residual trend (ºC decade^{-1}). (i) Time series of SAT anomalies (black), relative contributions due to circulation changes (blue) and residuals (red) over Europe and linear trends (ºC decade^{-1}; numbers in top right). The circulation index used for decomposition of SAT trends is the height index, which is defined as the area averaged geopotential height over the region (40ºN-65ºN, 5º-50ºE, black box in c and f) with zonal averaged value over the same latitude band removed (see Methods). The global mean is removed in panels (a-h) and the removal of global mean has a very little impact on panels (b-g). Note that nonlinear color bar is used in all spatial patterns. The red box in (b) and (e) is used to define a zonal jet index over the Mediterranean to test the sensitivity of SAT trend decomposition over Europe to an alternative choices for the circulation index and results are shown in Supplementary Information Figure S4.

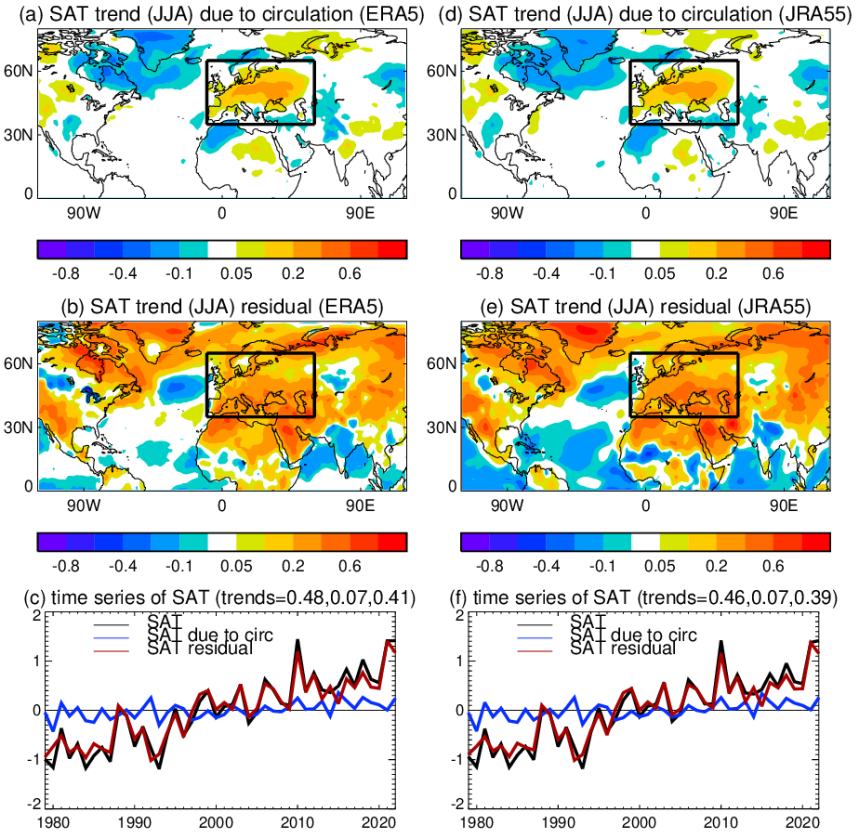

Supplementary Fig. S5: Linear trends of SAT due to circulation changes (based on a zonal wind index) and SAT residual trend in JJA during 1979-2022. (a, d) SAT due to circulation changes (ºC decade^{-1}), (b, e) SAT residual trend (ºC decade^{-1}), and (c, f) time series of SAT anomalies (black), relative contributions due to circulation changes (blue) and residuals (red) over Europe and linear trends (ºC decade^{-1}; numbers in top right). (a, b, c) ERA5 reanalysis and (d, e, f) JRA55 reanalysis. The global mean is removed in panels (a-e) and the removal of global mean has a very little impact on panels (a, e). Note that nonlinear color bar is used in spatial patterns (a-e). The circulation index is zonal index averaged over the Mediterranean (35ºN-50ºN, 0º-50ºE) at 500 hPa which is outlined in red box in panels (b, e) in Fig. 3. The black box outlines the region that is used to define SAT index over Europe. The details for decomposition of SAT trends are in Methods.

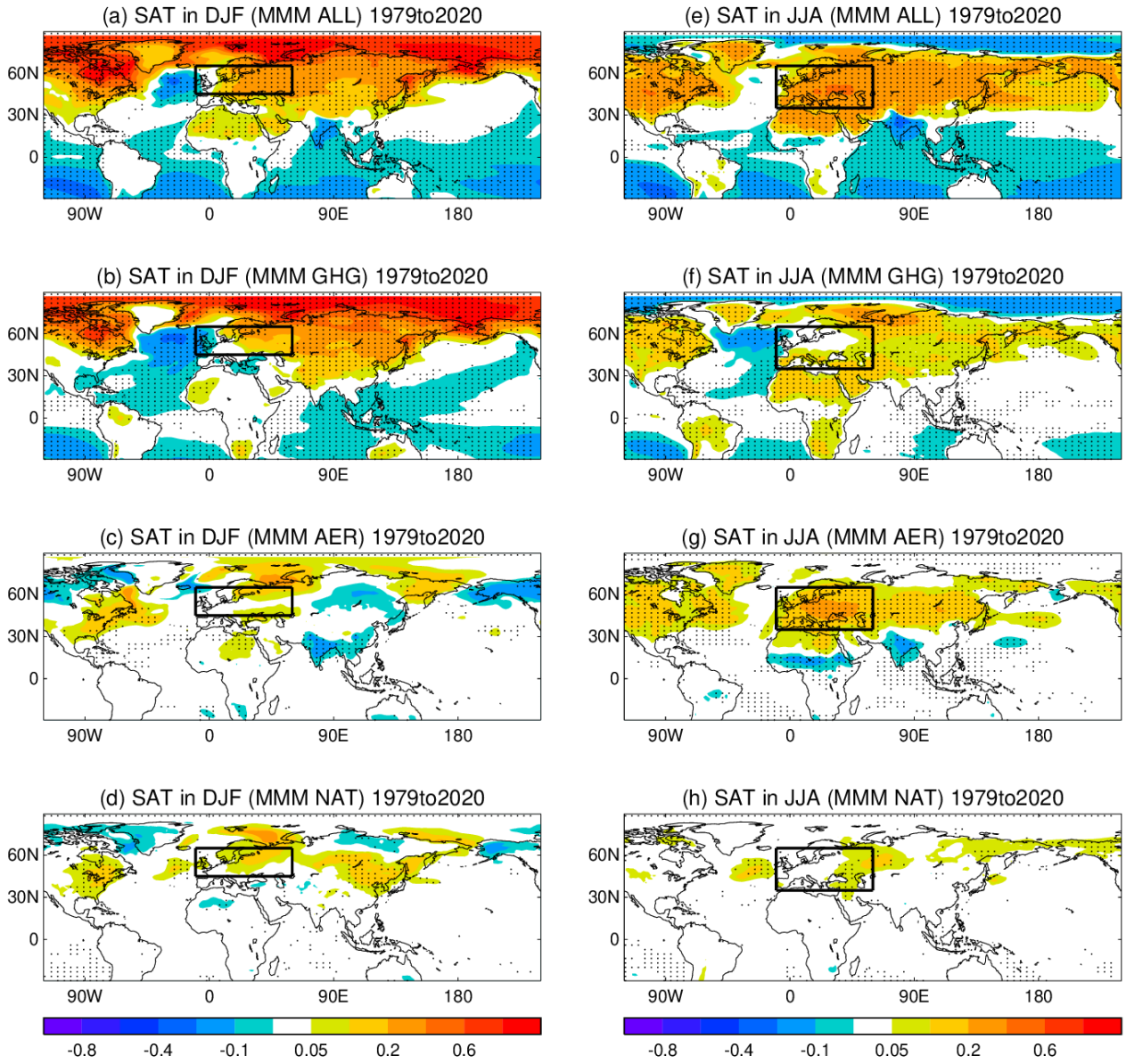

Supplementary Fig. S6: The multimodel mean (MMM) linear trends of SAT (^{o}C decade^{-1}) in winter (December, January, February) and summer (June, July, August) during 1979-2020 in CMIP6 historical extended (DAMIP) simulations with the global mean trend removed. (a, b, c, d) Response to different forcings (ALL, GHG, AER, NAT) in DJF and (e, f, g, h) in JJA. Dots indicate regions where 80% of models have the same sign of trend. Note that nonlinear color bar is used in spatial patterns. The black box outlines the region that is used to define SAT index over Europe. The details for analyses of model simulations are in Methods.

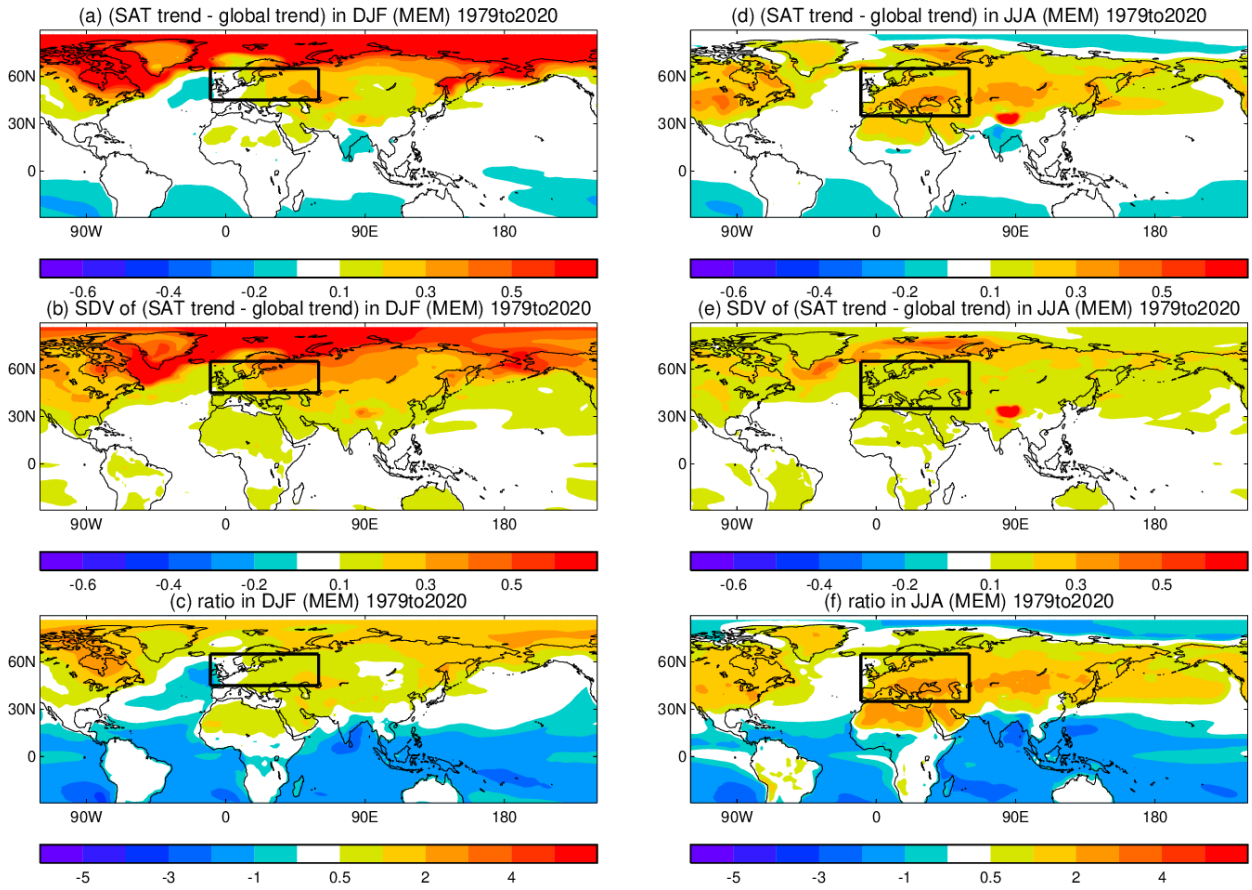

Supplementary Fig. S7: The multi-ensemble mean (MEM) excess warming trends of SAT (ºC), inter-ensemble standard deviation, and their ratio in winter (December, January, February) and summer (June, July, August) based on CMIP6 historical extended simulations during 1979-2020. (a, d) MEM SAT trends in winter and summer. (b, e) corresponding standard deviations. (c, f) ratios of MEM excess warming relative to standard deviations. The black box outlines the region that is used to define SAT index over Europe.

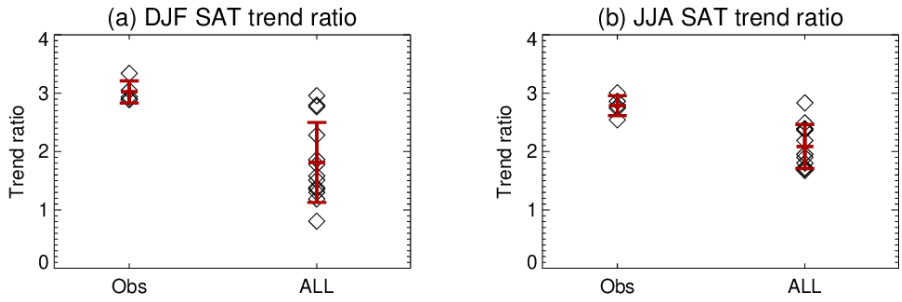

Supplementary Fig. S8: Warming ratios of linear trends of SAT indices over Europe relative to global mean in winter (December, January, February) and summer (June, July, August) in observations/reanalyses and CMIP6 historical extended (DAMIP) simulations. Ratios for observations/reanalysis are calculated during 1979-2022 and for all models are calculated during 1979-2020 based on CMIP6 historical model simulations. Ratios from each observations and individual models are represented with diamonds. The pluses show the multi-data set mean or the multi-model mean and red lines indicate one standard deviation range among all models. The details are in Methods.

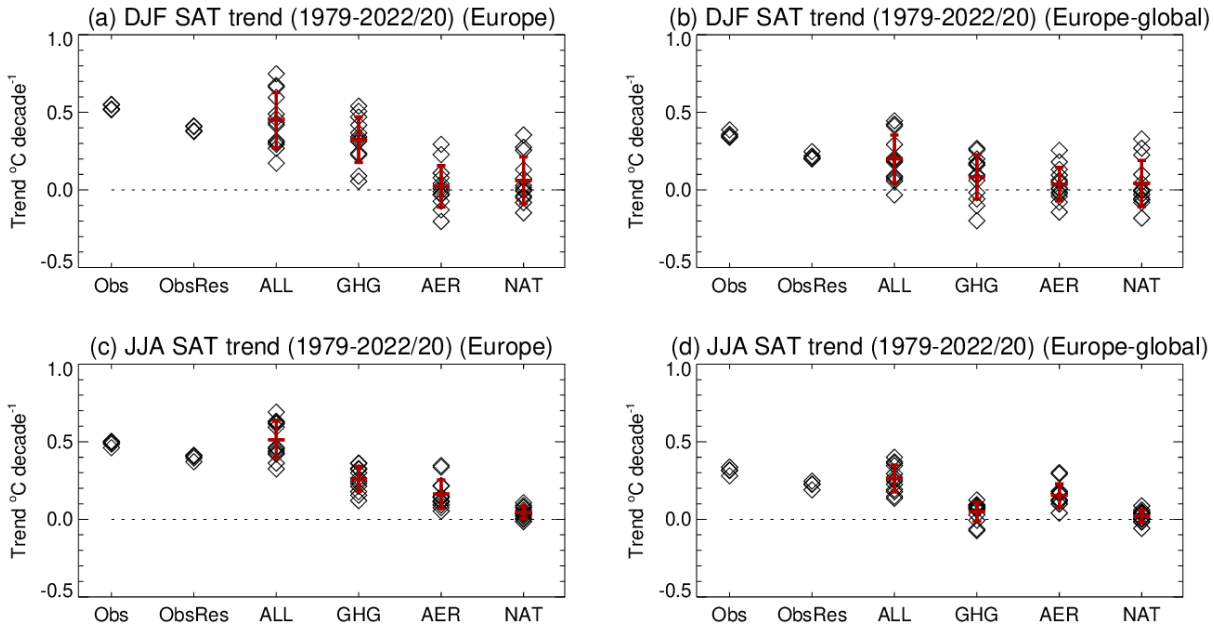

Supplementary Fig. S9: Linear trends of SAT indices in winter (December, January, February) and summer (June, July, August) in observations/reanalyses and CMIP6 historical extended (DAMIP) simulations. (a, c) SAT (ºC decade^{-1}) over Europe and (b, d) SAT trend difference between Europe and global mean in each of observations/reanalysis during 1979-2022 and all models during 1979-2020 based on CMIP6/DAMIP model simulations in response to different forcings. (a, b) for DJF and (c, d) for JJA. ObsRes is the SAT residual trend with the circulation induced trend based on ERA5 reanalysis removed from the total SAT trend. Trends from each observations and individual models are represented with diamonds. The pluses show the multi-model means and red lines indicate one standard deviation range among all models. The details are in Methods.

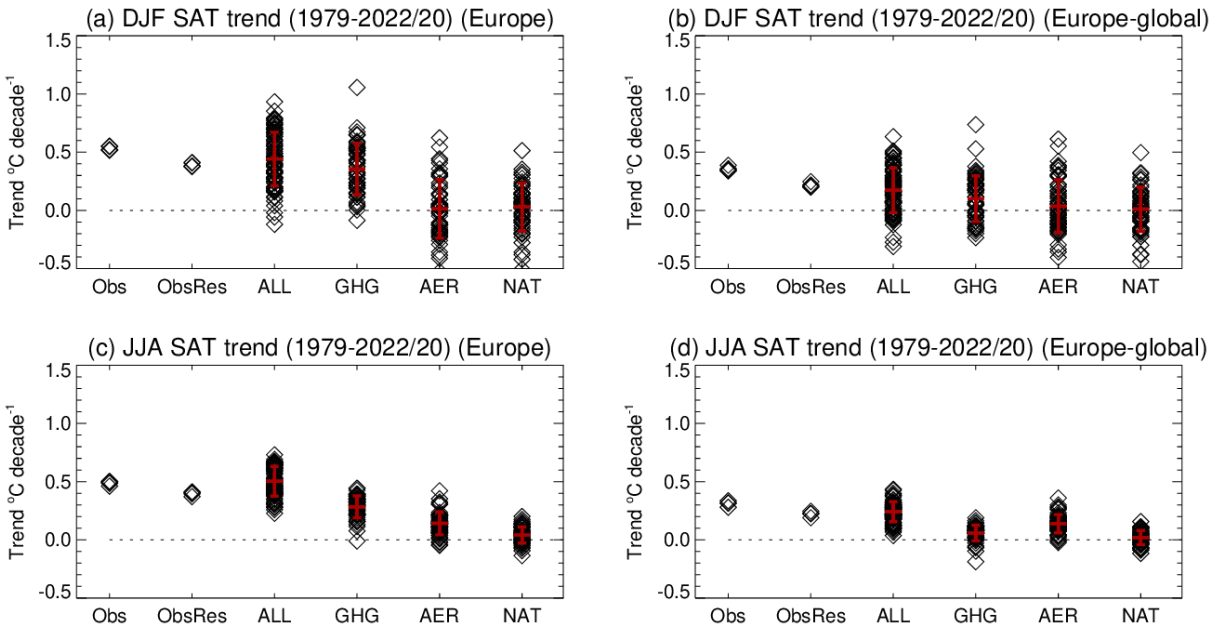

Supplementary Fig. 10: Linear trends of SAT indices in winter (December, January, February) and summer (June, July, August) in observations/reanalyses and CMIP6 historical extended (DAMIP) simulations. (a, c) SAT (°C decade^{-1}) over Europe and (b, d) SAT trend difference between Europe and global mean in each of observations/reanalysis during 1979-2022 and all model ensembles during 1979-2020 based on CMIP6/DAMIP model simulations in response to different forcings. (a, b) for DJF and (c, d) for JJA. ObsRes is the SAT residual trend with the circulation induced trend based on ERA5 reanalysis removed from the total SAT trend. Trends from each observations and individual members are represented with diamonds. The pluses show the multi-ensemble means and red lines indicate one standard deviation range among all ensemble members. The details are in Methods.

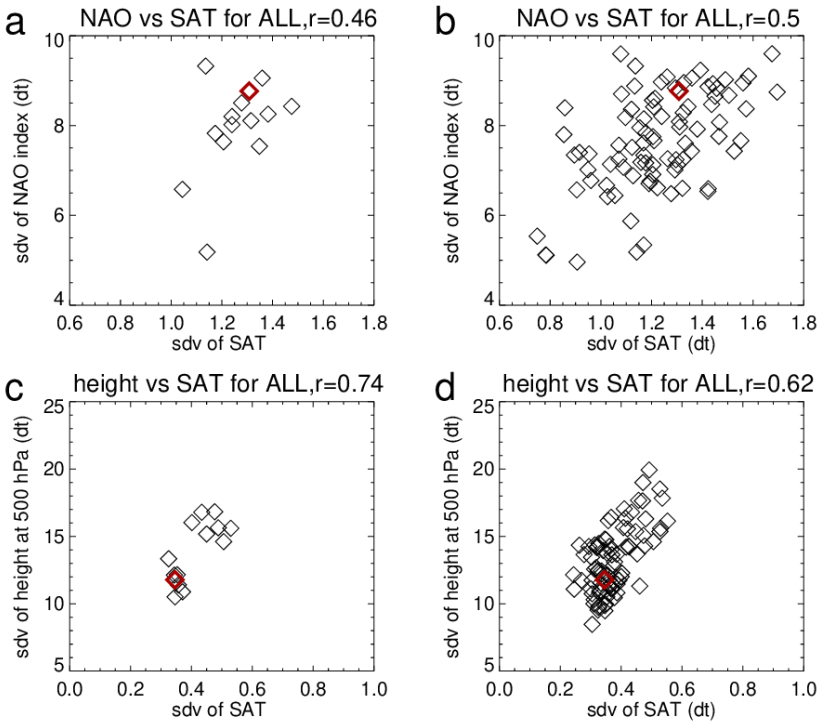

Supplementary Fig. S11: Relationships of between standard deviations of the area averaged SAT (ºC) over Europe with standard deviations of circulation indices in DJF and JJA during 1979-2020 based on CMIP6 historical extended (ALL forcing) simulations. (a, b) Standard deviations of the area averaged SAT (ºC) over Europe with standard deviations of NAO index. (c, d) Standard deviations of the area averaged SAT (ºC) over Europe with standard deviations of the area averaged height (m) at 500 hPa over Europe. The indices are calculated with detrended data. (a, c) for ensemble mean for each model, and (b, d) for all members of all models. The red symbol is based on ERA5 reanalysis.

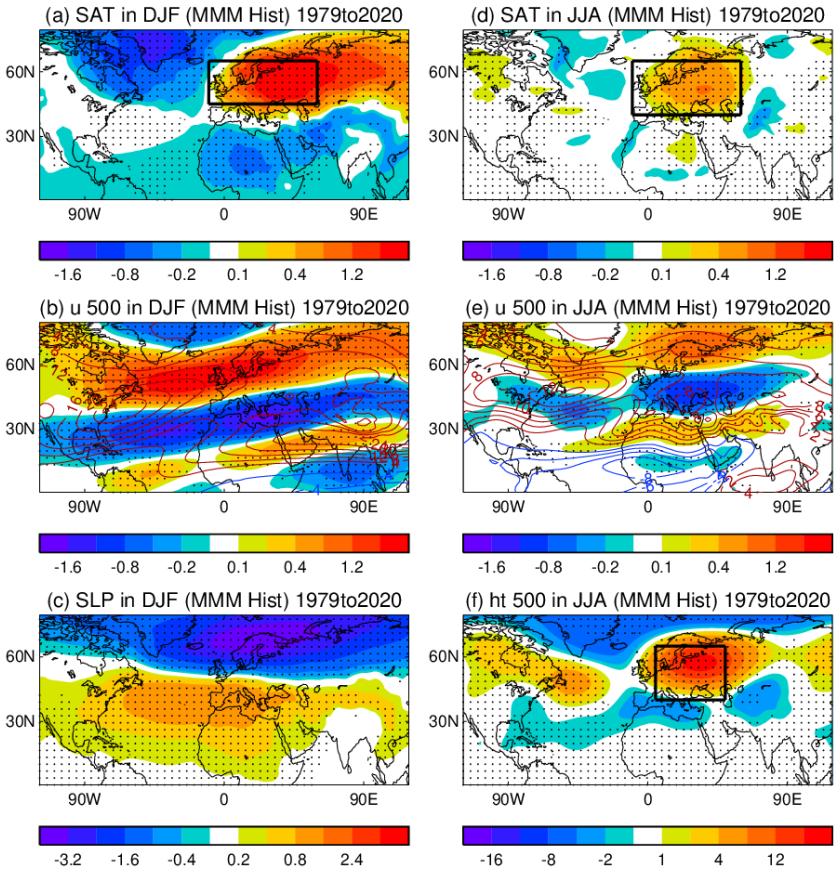

Supplementary Fig. S12: The multimodel mean (MMM) regression patterns of SAT and circulation in DJF and JJA to the normalized time series of the European SAT index based on CMIP6 multi-model historical extended (ALL forcing) simulations during 1979-2020 with detrended data. (a, b, c) MMM regression patterns of SAT (ºC), zonal wind (m s^{-1}) at 500 hPa, and (c) SLP (hPa) in DJF to the normalized time series of the European SAT index in DJF. (d, e, f) MMM regression patterns of SAT (ºC), zonal wind (m s^{-1}) and geopotential height (m) at 500 hPa in JJA to the normalized time series of the European SAT index in JJA. The global mean is removed in all panels and the removal of global mean has a very little impact. Note that nonlinear color bar is used in spatial patterns. The indices and regression patterns are calculated with detrended data. Dots indicate regions where 80% models have the same sign of regression. The black box in (a, b) outlines the region that is used to define SAT index over Europe and that in (f) outlines the region that is used to define geopotential height index. The details for analyses of model simulations are in Methods.

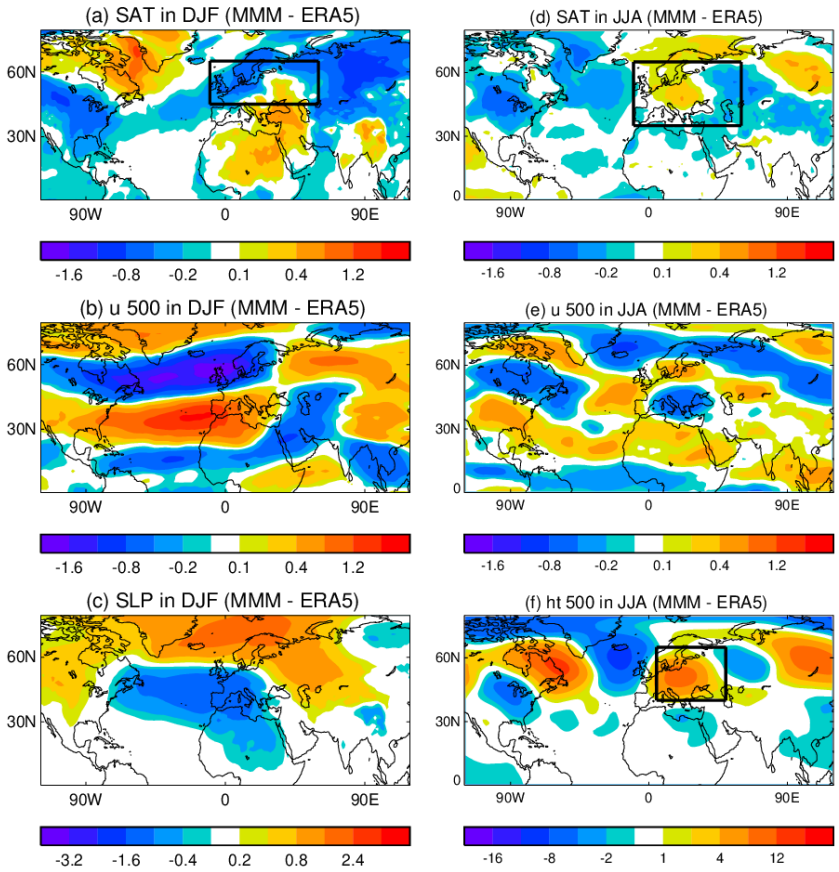

Supplementary Fig. 13: The differences between the multimodel mean (MMM) regression patterns of SAT and circulation in DJF and JJA to the normalized time series of the European SAT index based on CMIP6 multi-model historical extended (ALL forcing) simulations during 1979-2020 and those based on ERA5 during 1979-2022 with detrended data. (a, b, c) patterns of SAT (ºC), zonal wind (m s^{-1}) at 500 hPa, and (c) SLP (hPa) in DJF. (d, e, f) patterns of SAT (ºC), zonal wind (m s^{-1}) and geopotential height (m) at 500 hPa in JJA. Note that nonlinear color bar is used in spatial patterns. The black box in (a, b) outlines the region that is used to define SAT index over Europe and that in (f) outlines the region that is used to define geopotential height index. The details for analyses of model simulations are in Methods.

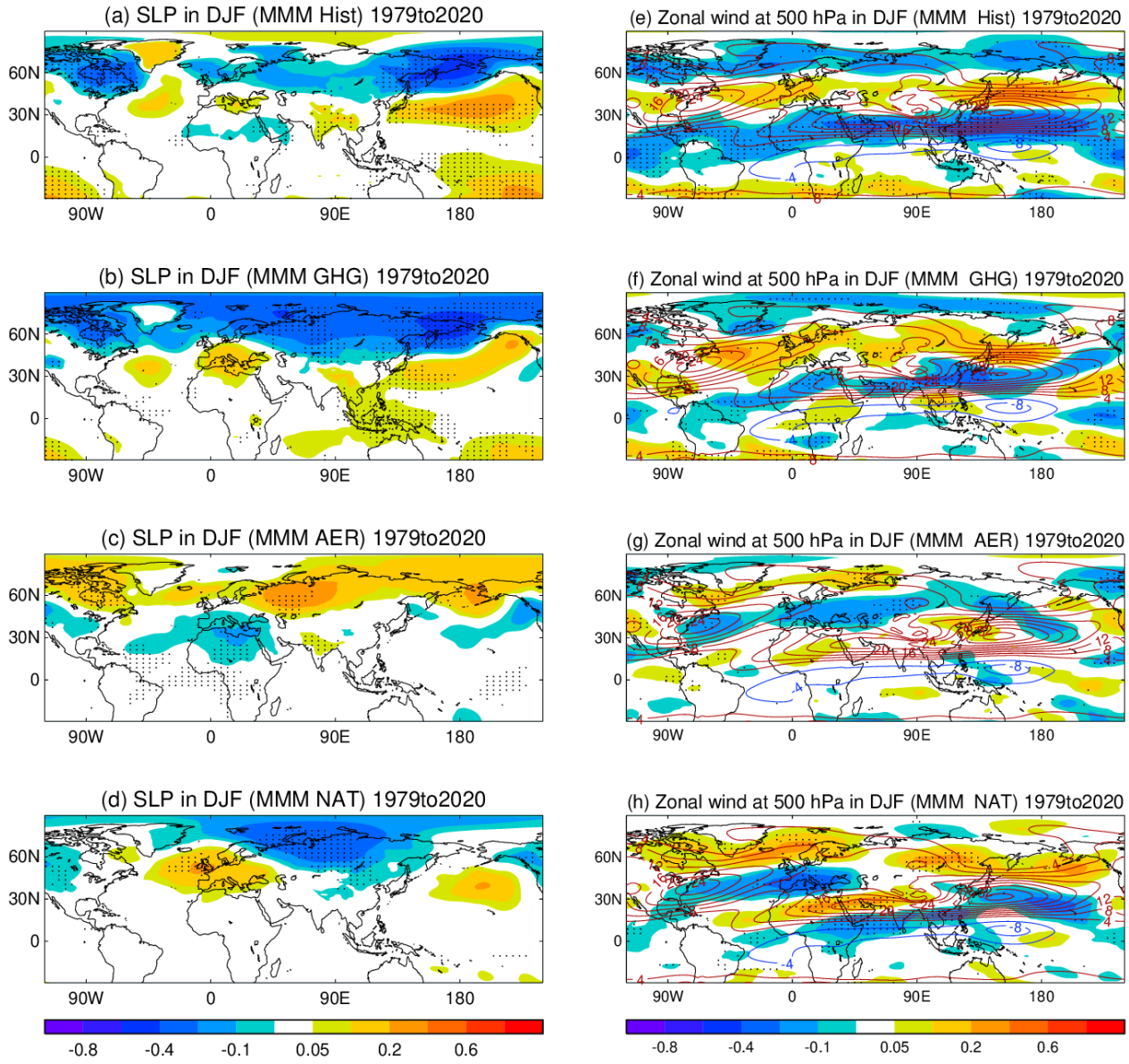

Supplementary Fig. S14: The multimodel mean (MMM) linear trends of SLP and zonal wind at 500 hPa in DJF during 1979-2020 based on CMIP6 historical extended (DAMIP) simulations. (a-d) SLP trends (hPa decade^{-1}) and (e-h) zonal wind trends (m s^{-1} decade^{-1}) at 500 hPa in response to different forcings (ALL, GHG, AER, NAT). Note that nonlinear color bar is used in spatial patterns. Dots indicate regions where 80% models have the same sign of trend. The details for analyses of model simulations are in Methods.

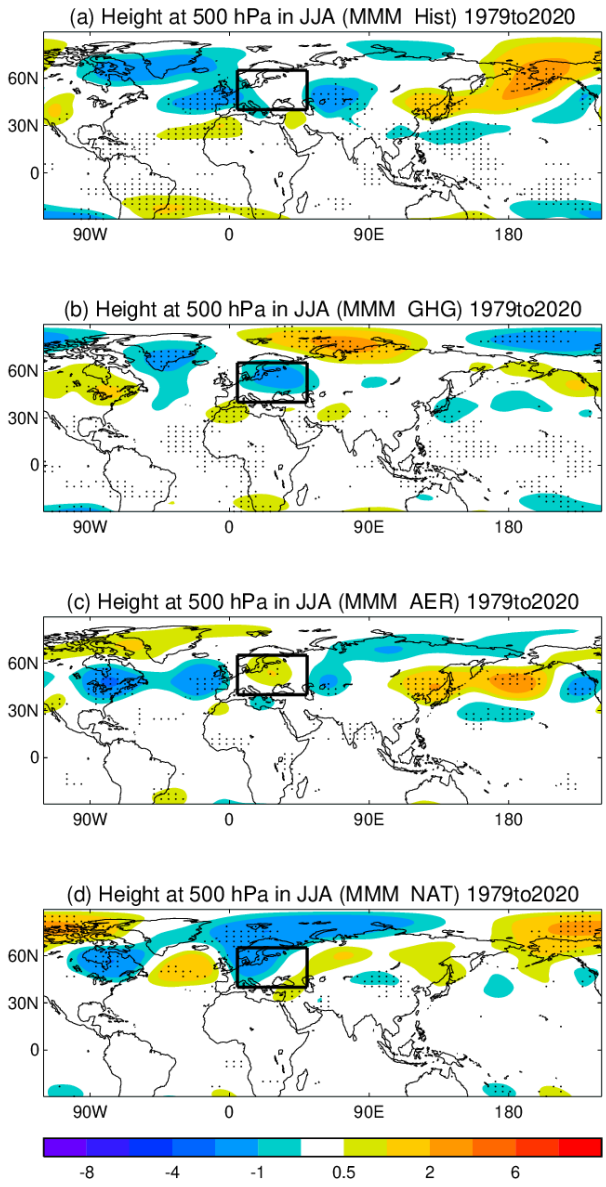

Supplementary Fig. S15: The multimodel mean (MMM) eddy component of geopotential height trends at 500 hPa during 1979-2020 in JJA based on CMIP6 historical extended /DAMIP model simulations. (a-d) Geopotential height trends (m decade^{-1}) in response to different forcings (ALL, GHG, AER, NAT). Note that nonlinear color bar is used in spatial patterns. Dots indicate regions where 80% models have the same sign of trend. The black box outlines the region that is used to define geopotential height index. The details for analyses of model simulations are in Methods.